Fluorescence transformation imaging

Irina-Mihaela Ciortan, Andrea Giachetti, Sony George, Jon Yngve Hardeberg

Irina-Mihaela Ciortan, Andrea Giachetti, Sony George, Jon Yngve Hardeberg, "Fluorescence transformation imaging," Proc. SPIE 11784, Optics for Arts, Architecture, and Archaeology VIII, 1178416 (20 June 2021); doi: 10.1117/12.2593651

SPIE.

Event: SPIE Optical Metrology, 2021, Online Only

Fluorescence Transformation Imaging

Irina-Mihaela Ciortan[a], Andrea Giachetti[b], Sony George[a], and Jon Yngve Hardeberg[a]

[a]Department of Computer Science, NTNU - Norwegian University of Science and Technology, Gjøvik, Norway
[b]Department of Computer Science, University of Verona, Verona, Italy

ABSTRACT

Fluorescent or luminescent materials absorb light at shorter wavelengths and re-emit at longer wavelengths. In terms of appearance, this translates to a increased color vividness, as well as a glowing effect. Thanks to these properties, the study of fluorescent materials is of interest for Cultural Heritage applications, where fluorophores are incorporated in many pigments and varnishes. This paper proposes a variant to Reflectance Transformation Imaging (RTI) technique, namely Fluorescence Transformation Imaging (FTI), that handles luminescent objects. Reflectance Transformation Imaging method outputs a single-camera multi-light image collection of a static scene, which can be used to model the reflectance of the scene as a polynomial of the illumination directions. Similarly, Fluorescence Transformation Imaging aims to model the fluorescent signal based on a series of images with fixed scene and viewpoint and varying incident light directions - what changes with respect to RTI is that fluorescence is recorded instead of reflected radiation. In the literature, there are works that explore the isotropic property of fluorescence in low-dimension multi-light imagery methods (such as Photometric Stereo) to model the appearance of an object with a first-order polynomial. This is based on the assumption that in the fluorescent mode the object gets closer to a Lambertian surface than in the reflective mode where non-Lambertian effects such as highlights are more likely to appear. Nonetheless, this assumption stands for single-object scenes, with uniform albedo and convex geometries. When there are multiple fluorescent objects in the scene, with concavities and non-uniform fluorescent component, then the fluorescence can become secondary light to the object and become a source of interreflections. Through quantitative and qualitative analysis, this paper explores the Reflectance and Fluorescence Transformation Imaging methods and the resulting texture maps towards appearance rendering of heterogeneous non-flat fluorescent objects.

Keywords: Fluorescence, Reflectance Transformation Imaging, Interreflections, Appearance Rendering

1. INTRODUCTION

Fluorescence is a photoluminescence phenomenon where light is absorbed at lower wavelengths and re-emitted at longer wavelengths. For classic artworks, this phenomenon is useful for detecting several resin-based aged varnishes or restorations. At the same time, modern artworks sometimes employ synthetic fluorescent pigments because of their special appearance properties. To name a few of these properties, highly bright and vivid colors that reflect more than the incoming light due to self-luminescence, as well as hidden details that gain visibility when illuminated by specific short-wavelength fluorescence-inducing light installations. For these reasons, fluorescent materials have received a lot of recent attention in the computer graphics and cultural heritage communities.

Nonetheless, fluorescent objects are challenging to measure, model and render. Due to the shift in the excitation-emission wavelengths they need to be measured by a bispectrometer, where for each illumination wavelength, the reflectance and emission response are recorded distinctly for each spectral band. The bispectral nature of fluorescent materials adds another layer of complexity to bidirectional reflectance distribution functions used in computer graphics to model the change in appearance with changing viewing angles and changing illumination angles. For this reason, most of the works make assumptions towards the type of fluorescence

Further author information: (Send correspondence to I.M.C.)
I.M.C..: E-mail: irina-mihaela.ciortan@ntnu.no

Optics for Arts, Architecture, and Archaeology VIII, edited by Haida Liang, Roger Groves, Proc. of SPIE
Vol. 11784, 1178416 · © 2021 SPIE · CCC code: 0277-786X/21/$21 · doi: 10.1117/12.2593651

exhibited by materials (uniform fluorescent composition, not reflecting the same color they fluoresce) to simplify the appearance modelling.

At the same time, Reflectance Transformation Imaging (RTI) has become an established multi-light image technique used for 2.5D reconstruction, appearance modelling and relighting with numerous active applications in the Cultural Heritage community.[1–5] The methods designed under the RTI umbrella have been tested for opaque and diffuse objects, as well as opaque and shiny surfaces. Even though there are a few works on using RTI for the rendering of translucent[6] and fluorescent materials,[7] the literature is still scarce on multi-light imagery of special materials. Moreover, for fluorescent materials, usually a low-dimensionality RTI stack of only 3-4 images has been investigated.[8,9]

This work aims to study the appearance of challenging scenes with fluorescent objects: with a heterogeneous distribution and concentration of fluorescent content; prone to interreflections by being reflective in the same wavelengths they fluoresce and by containing a mix of convex and concave geometries. For the study, single-camera multi-light images are collected with traditional Reflection Transformation Imaging and a proposed Fluorescence Transformation Imaging (FTI) method, and polynomial models are used to recover appearance coefficients.

2. RELATED WORK

Photometric Stereo and Reflectance Transformation Imaging. Photometric stereo was a method first proposed by Woodham et al.[10] for recovering shape from only few images acquired by a static viewpoint of a static object scene illuminated by different light directions. This pioneering work was aimed for Lambertian objects, that are diffuse and flat. The minimally optimal number of images to be acquired was defined as three, so that the linear system of equations composed by three unknowns (a coefficient for each of the x, y, z components of the light directions) can be overdetermined and uniquely solved. The coefficients in this case represent the components of the normal vector.

After photometric stereo was established as an image-based shape recovery technique, other models have been proposed as an improvement by relaxing the Lambertian assumption. In this sense, a groundbreaking work was the formulation of Polynomial Texture Maps (PTM) introduced by Malzbender et al.,[11] which fit a multi-light image collection to a quadratic polynomial, where instead of only the normal vector, 6 coefficients are reconstructed that account for the shape as well as other more complex non-Lambertian appearance phenomena: interreflections, shadow, highlights. Moreover, they coined a new term - Reflectance Transformation Imaging - as a general term for referring to the conversion of multi-light image collections to reflectance to maps that describe a surface appearance. In Drew et al.,[12] a modified second-order polynomial with different terms was proposed as an improvement to the original PTM[11] so that in case a purely Lambertian surface is captured, the three shape-related coefficients can be extracted from the model in a straightforward way without having to apply any non-linear operation to recover one of them, as it's the case with.[11] In addition, many robust methods have been designed to handle irregularities that break the Lambertian rule such as shadows and specularities.[12–14]

Fluorescence-based Photometric Stereo. One of the studies to empirically prove the isotropic property of fluorescence was carried out by Tominaga et al.,[15] where fluorescent samples were measured in a goniometric fashion. Their findings showed that the fluorescence radiance factor was changing with the variation of incident light with a trend very close to a cosine function, while there was little change with the viewing angles. The first works to exploit the Lambertian behaviour of fluorescence in a photometric stereo setup, completed by Treibitz et al.[8] and Sato et al.[9] were developed contemporarily. Both these works have similar findings. More precisely, they show that shape reconstruction from photometric stereo can be improved for fluorescent objects, because the specularities disappear in the fluorescent state making the surface more diffuse. They separate the fluorescent signal from the reflective signal through multispectral imaging. In,[8] a yellow filter is mounted on a trichromatic sensor to extract only the fluorescent signal excited by the blue light, while in,[9] they isolate fluorescence by working only with red and green channels. This assumption that fluorescence appears only in the red and green channels, exploited as well by Fu et al.[16] for developing an interreflection removal technique, is based on the physical properties of fluorescence of absorbing the light at lower wavelengths and re-emitting at higher wavelengths. However, this assumption perfectly stands in case of complete separation between the

sensitivites of the red, green and blue channels of the CCD sensors, while in the real case the trichromatic Bayer filter has broad-brand spread in the electromagnetic space. In addition, another aspect this assumption is that the fluorescence of the object has no overlap between the excitation and emission spectra, which is not true for all objects. The authors in[9] acknowledge this last considerations as limitation of their work. Moreover, they use it as justification for explaining why their method is prone to be less affected by interreflections: in their fluorescent state, materials with little to no overlap between their excitation and emission spectra are less likely to be excited by their own self-emission and thus, there are less mutual illumination effects in the fluorescent state than in the non-fluorescent reflective state. As pointed out by the authors in,[9] this is valid only for simple scenes containing only one objects. However, in more complex scenes with more objects with both concave and convex geometries, fluorescent components can become a second, indirect source of illumination for the scene. Especially if these materials reflect light in the same wavelengths where they fluoresce. Both[9] and[8] have minimized the problem of interreflection by studying simple scenes of materials that don't reflect the color they fluoresce. Under the same assumption, the work of[16] manages to decompose the direct and indirect illumination components from fluorescent images so that it later feeds the photometric stereo reconstruction only the interreflection-free direct light component images. Nonetheless, their approach requires homogeneous only materials.

To the best of our knowledge, Koutula et al.[7] are the only ones to have exploited the angularity of the light to visualize the relief of the fluorescent signal in museum ceramic artifacts. More precisely, Kotoula et al.[7] show the benefits of capturing reflectance transformation imaging in the UV-reflected (UVR) and UV-fluorescent (UVF) ranges for visualizing traces of conservation on two real ceramic vases from a museum. The filters proposed in their setup are off-the-shelf solutions for UV imaging: for the UVR, the UV-transmitter (HOYA 330) and IR barrier filter (SCHOTT BG 38); for the UVF, an UV and IR barrier filters were used (B+W 021). In the UVF RTI mode, traces of conservation, like previous repair of the ceramics become noticeable, because common adhesives are luminescent when lit by the UV light, revealing details otherwise obscure in the visible light. Actually, the authors in[7] argue that UVF RTI is basically an efficient way of recording a good practice of conservators when they visually inspect an artifact with UV light: they position the light around the artifact, at different raking lights and statically inspect the change in the appearance of the object at each distinct position of the light. In this way, UVF RTI becomes a way of documenting this process of dynamic inspection by stacking together all the static frames at each light direction into a single relightable file. In contrast with UVF, the UVR mode highlights the subtle variations in the surface, such as scratches and smudges, as well as traces remains of glaze and salt encrustations. Even though such variations might be revealed as well in the visibile RTI, the contrast is enhanced under UV reflected light and the variations gain clarity. Therefore, the paper of[7] shows effectively how the combined forces of RTI and UV imaging can export visualizations and rendering useful for the analysis of Cultual Heritage objects.

3. MATERIALS AND METHOD

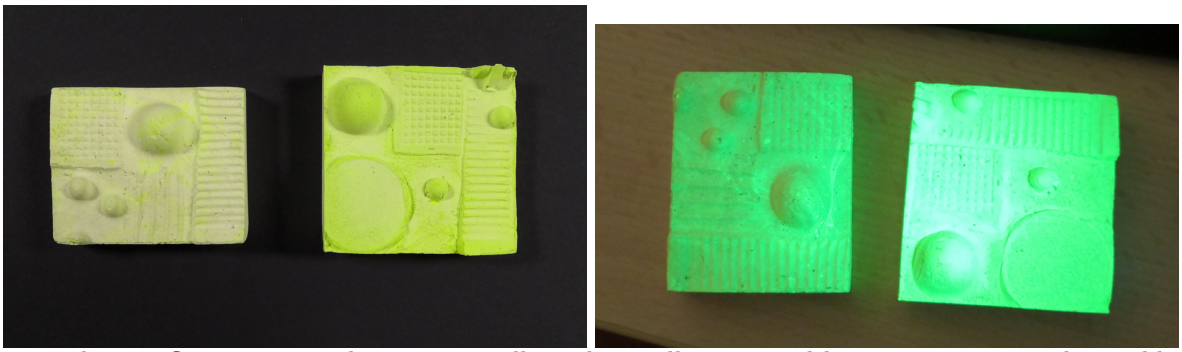

Figure 1: The two fluorescent mockups, as visually and casually inspected by a conservator under visible light and, respectively, ultraviolet light in uncontrolled conditions.

In this paper, we compare normal and appearance maps recovered with four representations of the Photometric Stereo model, based on multi-light image collections of two handmade fluorescent objects, shown in

Fig. 1. The fluorescent objects were designed to have complex convex and concave geometries, a heterogeneous composition and to reflect the same color as they fluoresce. The mockups are made of gesso mould mixed with a commercial UV-induced lime green, fluorescent pigment. One of the mockups has a higher overall concentration of the fluorescent pigment and the mixing was done in several iterations until achieving a more homogeneous material (referred to in the paper as highly fluorescent mockup). The other mockup contains a lower overall concentration of the fluorescent pigment and it is mixed in a rougher way, having a more heterogeneous composition (from now on, referred to in the paper as low fluorescent mockup). The two mockups were acquired with a multispectral light dome system in visible mode and fluorescent mode. Based on the two stack of images for each mode, surface normals and albedo maps are reconstructed using four methods. In the rest of this section, a brief theoretical background for these methods is outlined.

A multi-light image collection can be formalized as a system of linear equations, where on one side we have the intensity values and on the other side we have the polynomial based on the light direction vector. The terms and order of the polynomial depend on the assumptions made with respect to the surface appearance. In the case of classic Photometric Stereo (PS),[10] the assumption is that the material is perfectly Lambertian and the polynomial has a first-order and is modelled as follows:

$$anl = I_k \tag{1}$$

where a represents the albedo, n the normal, l the light direction vector, I the intensity and k the number of images taken at different illumination angle. If we split the light direction into the x, y, z components, and given that the albedo is a constant that can be computed as the norm of the normal vector, eq. 1 becomes:

$$n_{1k}lx + n_{2k}ly + n_{3k}lz = I_k \tag{2}$$

There are 3 unknowns so in order for the system to be determined and reach a unique solution, at 3 equations are needed, given by the capture of 3 intensity images under varying light directions. To ensure accuracy, common practice is to acquire more than 3 images, where the overdetermined system is solved with Least-Squares regression.

Since most of the real-world objects are not perfectly Lambertian, the reconstruction of albedo and normal maps with classic Photometric Stereo is affected by more complex appearance effects such as specularities, shadows or interreflections. Many methods that were proposed to extend this limitation focus on extending the number of parameters of the surface model and/or design robust strategies for solving the system of equations. The increased complexity of the models requires a higher number of images and hence, a multi-light image collection. One of the first methods to extend the classic Photometric Stereo, by increasing the number of modelled coefficients other than normal and albedo, PTM,[11] replaced the first-order polynomial with a second-order polynomial. This results in the recovery of 6 appearance descriptor maps.

One constraint of the PTM polynomial is that in case the analyzed object has a subset of its surface that is perfectly Lambertian, then the regression of the biquadratic polynomial will not directly output the normal vectors. This limitation is accounted for by the modified polynomial terms proposed by Drew et al. (PTMD) in:[12]

$$c_{1k}lx + c_{2k}ly + c_{3k}lz + c_{4k}lxly + c_{5k}lz^2 + c_{6k} = I_k \tag{3}$$

where $lz = \sqrt{1 - lx^2 - ly^2}$ and the normal vectors are given by the first three coefficients. Simultaneously with the straightforward recovery of the normal vectors for Lambertian parts, PTMD models as well high-frequency and low-frequency non-Lambertian components (4th and 5th coefficients). However, the distinction between the nature of these components (highlights, interreflection, shadows) is not trivial.

Furthermore, the influence of the outliers can be accounted for with robust fitting strategies that solve the system of equations bypassing the Least Squares method. For instance, one such approach reformulates the regression problem as the task of matrix rank minimization,[14] assuming that the full set of observations explains the Lambertian component of the material with a low-rank matrix and the outlier with a sparse matrix. In

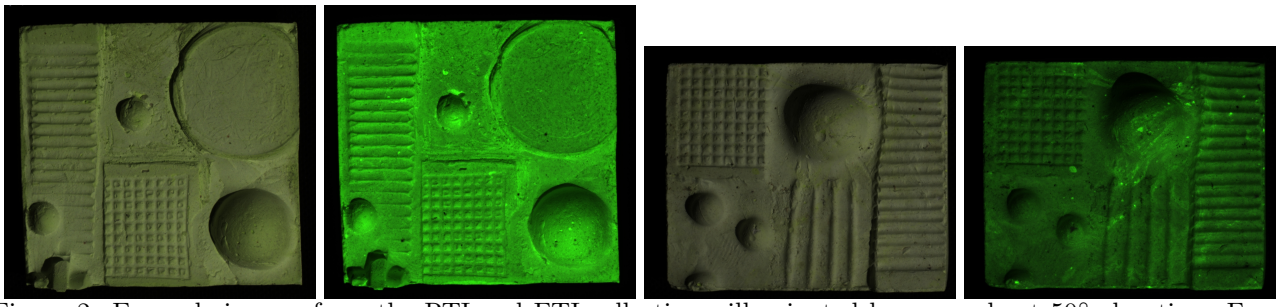

Figure 2: Example images from the RTI and FTI collections, illuminated by an angle at 50° elevation. From left to right: mockup with higher and almost uniform fluorescent component in the reflective, then fluorescent mode; mockup with lower and heterogeneous fluorescent component in the reflective, then fluorescent mode.

addition, a per-pixel estimation of the light directions, was proved to be more effective at estimating surface normals with polynomial models as opposed to assuming a constant light direction for all the scene.[17]

In the experimental part of our paper, we discuss the results obtained with four variants of the classic Photometric Stereo algorithm: the first-order polynomial in Eq. 1, with constant light direction vector and solved with Least-Squares; the first-order polynomial in Eq. 1, with constant light direction vector and solved with low-rank matrix minimization;[14] the second-order polynomial in Eq. 1, with per-pixel light direction vector and solved with Least-Squares; the second-order polynomial in Eq. 3 with per-pixel light direction and solved with Least-Square.

4. RESULTS

4.1 RTI and FTI Data Acquisition

The two fluorescent mockups that contain impressions of convex spherical objects as well as concave patterns were acquired with a multispectral RTI light dome,[4] with lights distributed at different elevation (50°, 30° and 10°) and azimuth angles. The ambient light was controlled by covering the dome in black non-reflective clothing. The sensing device was a Nikon D810 RGB camera, with a 50 mm lens. The objects were captured in two modes (see Fig. 2): reflective mode, under visible light (illuminated by white LEDs), and fluorescent mode, under ultraviolet light (illuminated by ultraviolet LEDs) in combination with a filter attached to the camera that separates the fluorescent signal from the UV-reflected signal.

Because filtering individually the visible radiation emitted by each UV LED was impractical, we tested different filters assembly for filtering the UV-reflected radiation during the fluorescence analysis. Fig. 3 shows the normalized transmittance curves of the measured filters compared with the spectral power distribution of the UV LEDs of the dome as reported by the manufacturer. Hoya Pro1Digital UV filter was used for blocking the internal fluorescence of the tested coloured filters: Nikkon Y44 and Hoya K2. Hoya K2 filter was chosen for the experiments reported in this paper, cuts wavelengths lower than 500 nm, filtering most of the visible emission tail of the UV LED.

At each light direction, a picture was shot sequentially, in the visible and fluorescent modes.The multi-light image collections were converted from the raw signal to linear tiff using dcraw. Afterwards, the stacks of images were processed with RTItool,[18] where firstly, geometric undistortion was applied. Then, the light-direction vectors were recovered assuming a perspective projection based on the semi-automatic annotation of the calibration targets (4 glossy spheres). Given the polygonal arrangement of the 4 spheres (enclosing the object), an interpolation was made between the 4 light direction vector and so, the light directions were locally estimated for each pixel in the image. In addition to the per-pixel light direction, a constant light direction for all image can be computed as the average of the 4 light direction vectors estimated from the 4 spheres. Finally, an appearance profile is generated for the two mockups, where for each pixel, the color information is encoded for each light direction.

Once the appearance profile is obtained, the surface coefficients are recovered with four fitting models: classic Photometric Stereo, with constant light direction and Least-Squares fitting (PS-L2),[10] Photometric Stereo with

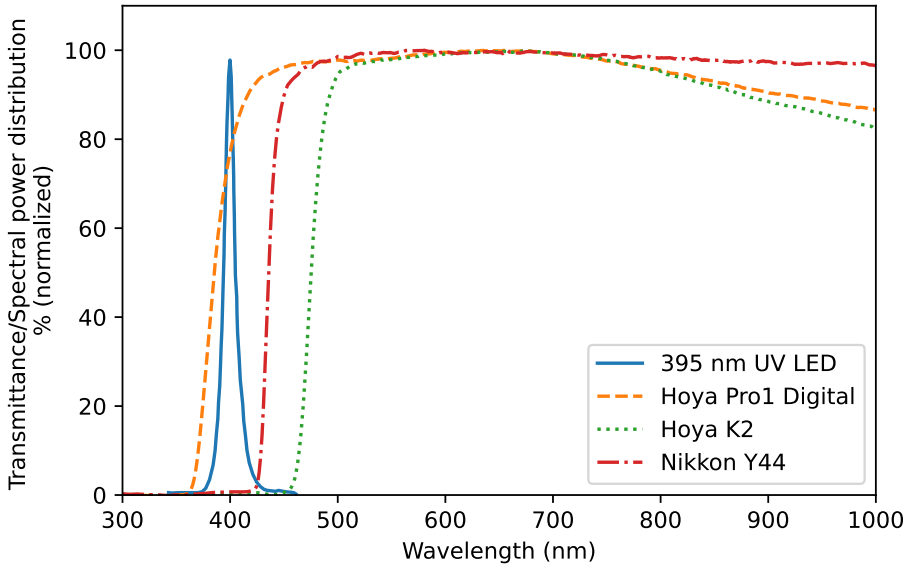

Figure 3: Normalized transmittance curve measured for off-the-shelf fluorescence-pass filters, together with the spectral distribution of the UV LED light of the dome.

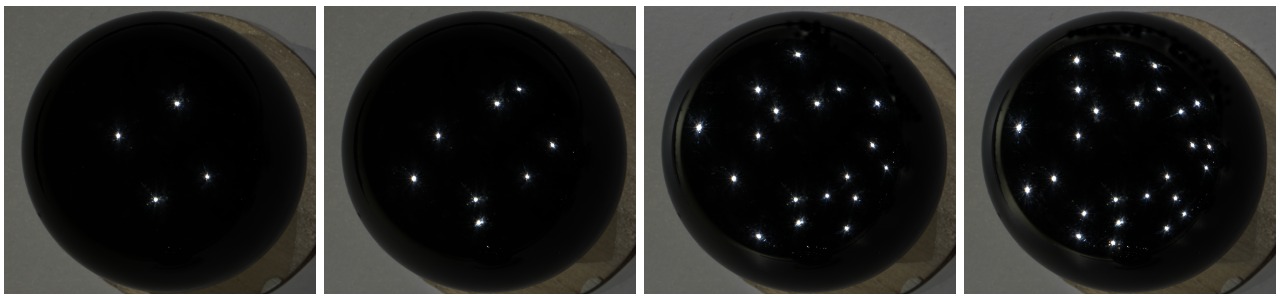

(a) 1 (4 lights) (b) 2 (8 lights) (c) 3 (18 lights) (d) 4 (26 lights)

Figure 4: We use four different light distributions to evaluate the quality of the Reflectance and Fluorescence Transformation modes. As mirrored on the reflective sphere, in each of the four distributions, the lights are sampled in approximately radially symmetric way.

per-pixel light direction and Least-Squares fitting (PS-4-L2), Photometric Stereo based on low-rank matrix minimization (PS-RPCA),[14] Polynomial Texture Maps with Drew terms[12] with per-pixel light direction and Least-Squares fitting (PTMD-4-L2). The fitting is performed based on various light distributions (see Fig. 4) in order to investigate the impact of the number of light directions and their spatial arrangement on the quality of appearance reconstruction. The 4 light constellations are sampling increasing number of lights at different elevation angles with approximately opposite azimuth distancing.

4.2 Ground-truth Shape Scanning and Registration

In order to compare the surface normals maps estimated with RTI and FTI, we scan the shape of the mockups with an off-the-shelf structured light 3D scanner.[19] Once the mesh of the surfaces is recovered, we align the two coordinate systems using mutual information algorithm[20] as implemented in Meshlab.[21] Mutual information algorithm optimizes the roto-translation matrix in an iterative fashion based on the statistical similarity between the normal map obtained with the camera (from RTI anf FTI modes) and various renderings of the 3D model (normal map, ambient occlusion map and specular map). After alignment has converged, the 3D model is

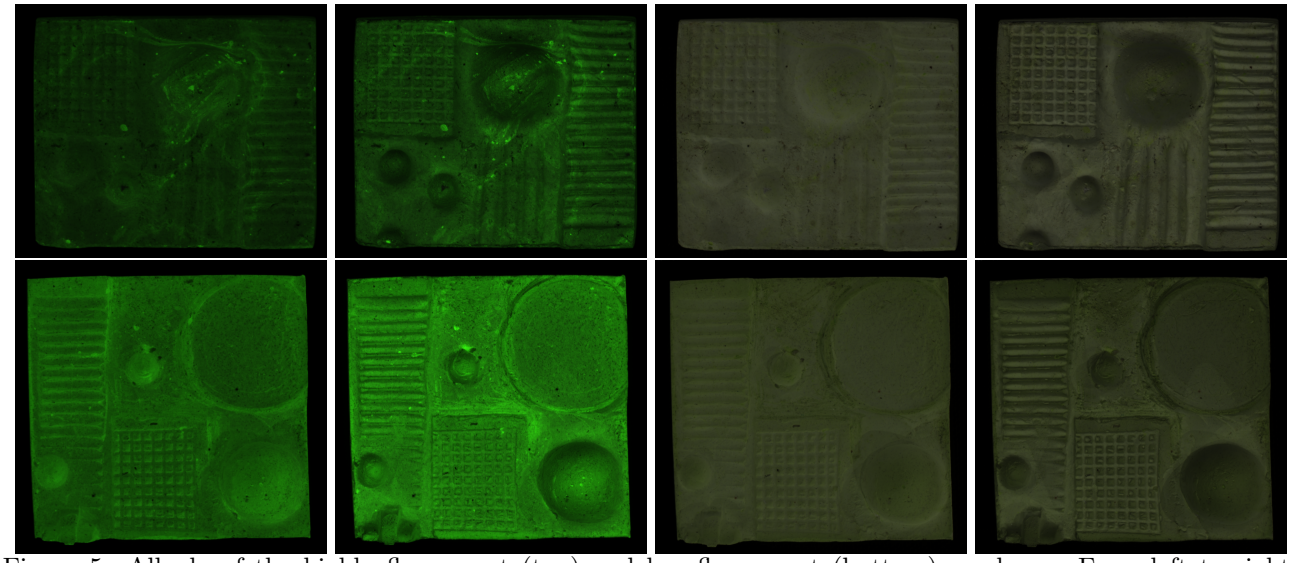

Figure 5: Albedo of the highly fluorescent (top) and low fluorescent (bottom) mockups. From left to right: reconstruction with FTI PS-4-L2, FTI PTMD-4-L2, RTI PS-4-L2, RTI PTMD-4-L2 for light configuration 4. The PS-4-L2 model seems to perform better at discarding the shading effects from the albedo map than PTMD-4-L2.

rendered with the camera parameters and the transformation matrix using Mitsuba renderer.[22] This protocol of shape-to-image alignment has been employed before in analogous task.[23,24]

4.3 Quantitative and Qualitative Analysis

Appearance maps, such as albedo and normal maps are recovered from the FTI and RTI multi-light image collections. The albedos of the two mockups reconstructed with PS-4-L2 and PTMD-4-L2 models in the fluorescent and visible modes are shown in Fig. 5. For both mockups, we can notice that the two models reconstruct a different albedo, while PS-4-L2 manages to better isolate the shading effects from the reflectance.

Surface normal maps given by RTI and FTI are compared with the normal maps derived from the 3D scans. Fig. 6 shows a visual comparison of the normal maps recovered with RTI next to the ground-truth ones. While the normal maps rendered from the 3D scanned models are overall sharper than the RTI surface normals, they present horizontal line artifacts. Moreover, in the highly fluorescent mockup, fine details of the coin imprint are better defined in the RTI surface normals. Even though the quality of the 3D scan normals is not impeccable, they still represent a common reference ground for comparison between the different RTI and FTI modes.

Angular difference is computed between the normal orientation vectors of ground-truth against those reconstructed with RTI and FTI as $arccos(n_{gt}^T n)$ for each of the 4 light distributions. The results are presented in the form of box-and-whiskers plots in Fig. 7 and 8, as well as difference maps in the Appendix A. Overall, the models that consider per-pixel light direction estimation show lower error than the models with constant light direction. Similarly, the former category exhibit more invariance to the change of number of lights than the latter.

For the low fluorescent mockup 7, the angular error is higher in the fluorescent mode than it is in the visible modes for all light configurations, as obtained with PS-L2, PS-RPCA and PS4-L2 models. The lowest median angular difference is given by the PTMD-4-L2 model, in particular for the 4^{th} light configuration with 10.95° for the visible mode and 11.46° for the fluorescent mode. Nevertheless, there is a general high overlap between the distributions of the angular error difference in visible or fluorescent modes, meaning that the difference between the two modes is not significantly large for this object. The impact of the light distribution varies according to the fitting model, but is constant between fluorescent/visbile modes: for PS-L2 and PS-RPCA, it seems that the best light configuration is configuration 2 (8 lights), while for per-pixel methods, PS-4-L2 and PTMD-4-L2,

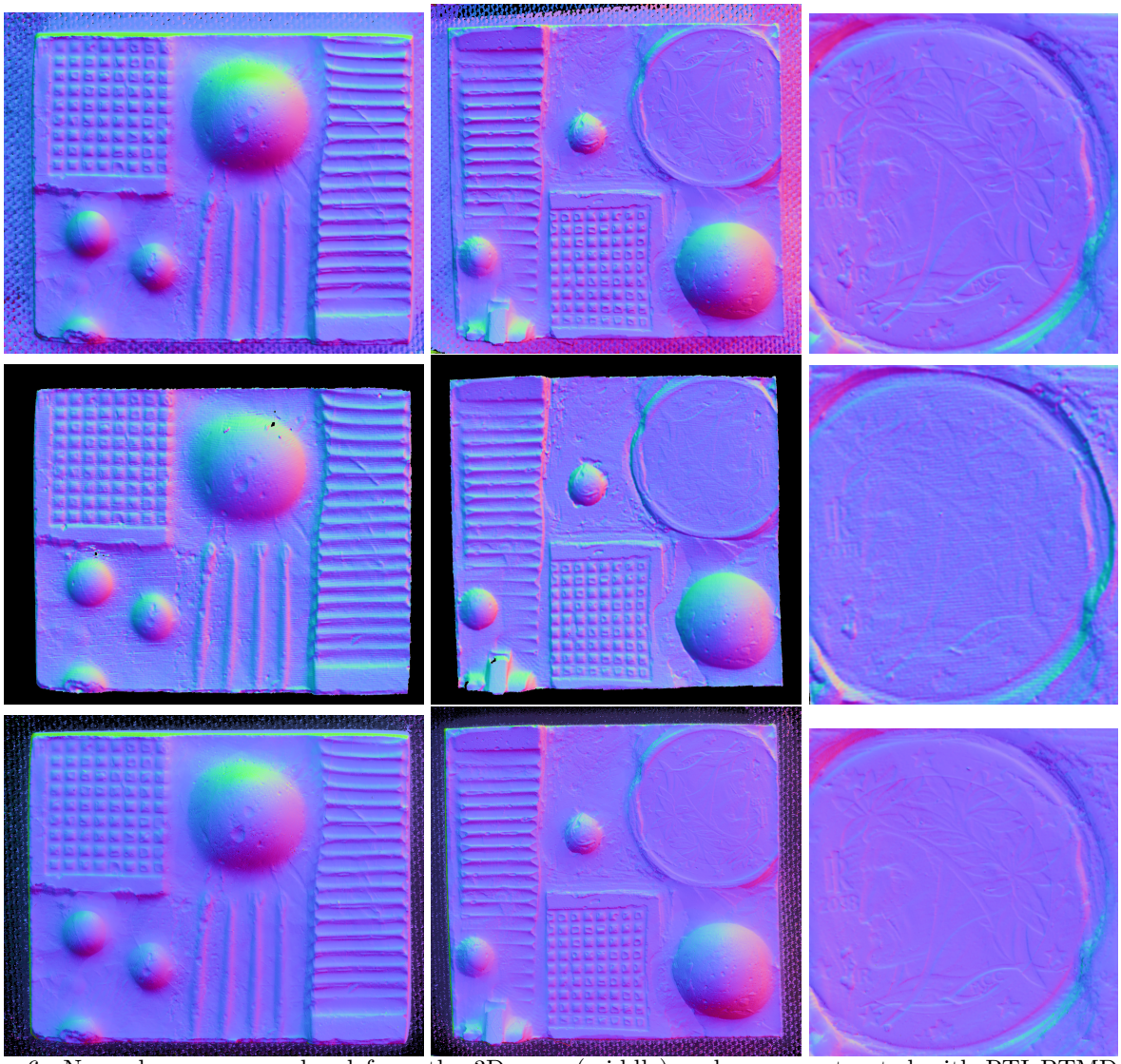

Figure 6: Normal maps as rendered from the 3D scan (middle) and as reconstructed with RTI PTMD-4-L2 (top) and FTI PTMD-4-L2 (bottom) based on light configuration 4. From left to right: low fluorescent mockup, highly fluorescent mockup, rotated detail of the coin imprint from the right upper corner of the highly fluorescent mockup. The RTI and FTI normal maps manage to render fine elements of the coin imprint (such as the issue year and the contours of the portrait) more accurately than the 3D scan. Nonetheless, they have poorer estimation for the elements with higher depth.

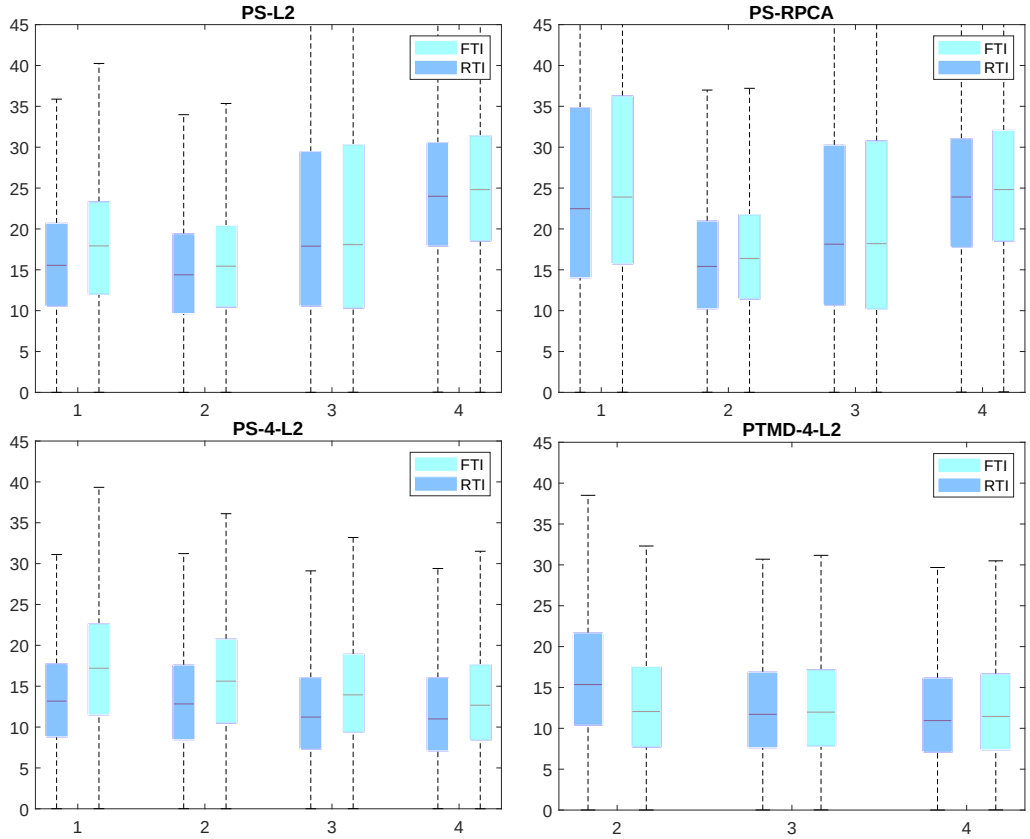

Figure 7: Angular error in degrees (Y-axis) between the ground-truth normal of the low fluorescent mockup and the normals reconstructed with RTI and FTI methods with varying light distributions (X-axis). The angular errors were computed only for the area corresponding to the object, background was discarded.

configuration 4 (26 lights). It is noteworthy to point out that in the fluorescent mode, PTMD-4-L2 seems to be more stable across varying light distributions than it is the case for the visible mode.

The differences between visible and fluorescent modes are more salient for the highly fluorescent object. Similar to the low fluorescent case, the higher angular differences correspond to the fluorescent mode. Moreover, this time, given the lower extent of the overlap between the two distributions, the discrepancy between visible and fluorescent modes is more significant. For the visible mode, the lowest angular error is provided by the PS-4-L2 and 4th light configuration with a median value of 9.12°, while for the fluorescent mode the lowest median angular difference is 17.82° given by the PTMD-4-L2 and the same 4^{th} light configuration. A descending trend is observed for the error as the number of lights increases, which stops at the the 3^{rd} light distribution for PS-L2 and PS-RPCA, while continues up until the 4^{th} light distribution for PS-4-L2 and PTMD-4-L2.

The fact that, for the given case studies, higher errors correspond to the normals recovered in the fluorescent mode contravene the expectation given by previous findings in the scientific literature[8,9] where due to its presumable isotropic property, fluorescence is more accurately approximated by the classic photometric stereo model than signal in the visible light reflective mode. Moreover, the modulation of the angular error with varying light distributions in the fluorescence mode further indicates the presence of deviations from a perfectly Lambertian behaviour. It is true that in[8] and,[9] they exploit the fluorescence mode for objects that are highly specular in the visible mode, while in our case, the objects are diffuse in the visible mode. In addition,[8] and[9] work with single-geometry scenes and objects with uniform albedo that don't fluoresce the same color they reflect, ensuring the lack of interreflections provoked by the luminescence becoming a secondary light source in the scene. We specifically designed our mockups to break the above-mentioned assumptions. The results of our proposed experiments imply that heterogeneous, non-flat and cluttered fluorescent scenes exhibit more non-Lambertian

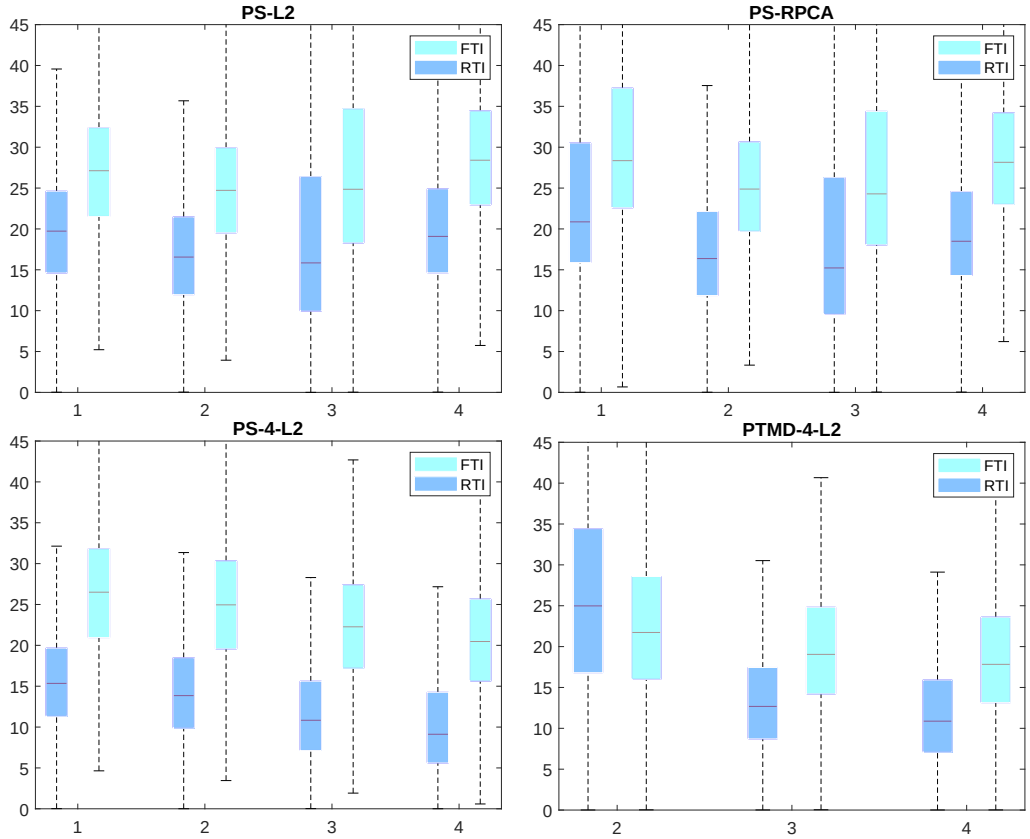

Figure 8: Angular error in degrees (Y-axis) between the ground-truth normal of the highly fluorescent mockup and the normals reconstructed with RTI and FTI methods with varying light distributions (X-axis). The angular errors were computed only for surface corresponding to the object, background was discarded.

effects in the fluorescent mode. This might be partly explained by the higher number of interreflections provoked by the luminescence becoming a secondary light that gets reflected by the object (that both reflects and emits green color).

In an attempt to further assess the presence of non-Lambertian effects in the mockups, we visually compare the 4^{th}, 5^{th} and 6^{th} coefficient maps in Fig. 9 of the PTMD-4-L2 polynomial, as expressed in Eq. 3, for the Green color channel, which is the most relevant for investigating the cross-signal between fluorescence and visible reflectance. The 6^{th} is the constant, ambient term, while the 4^{th} and 5^{th} coefficients model non-Lambertian high and low frequency effects such as highlights, interreflections and shadows. However, it is not obvious and immediate how to separate between the various effects. Nonetheless, we can notice that these non-Lambertian effects are present in visible mode and are definitely not lacking in the fluorescent mode. Moreover, since the mockups reflect the color that they emit in fluorescence mode, we expect that the mutual illuminations effects are higher in the fluorescent mode. Indeed, the green channel of the 4^{th} and 5^{th} PTMD-4-L2 coefficients show more variation in the fluorescent mode than for the visible mode in the case of the high fluorescent mockup. This is valid for the low fluorescent mockup, spread of differences is overall lessened and more limited to certain areas like edges and concavities.

However, in order to find out the precise nature and cause of higher angular errors for the normal maps in the fluorescence method, further investigation is needed, and ideally, validated with synthetic data, where ground-truth with respect to each outlier (shadows, interreflections and highlights) are known in advance and can be discarded from the pipeline. We plan to explore these aspects in-depth in future work.

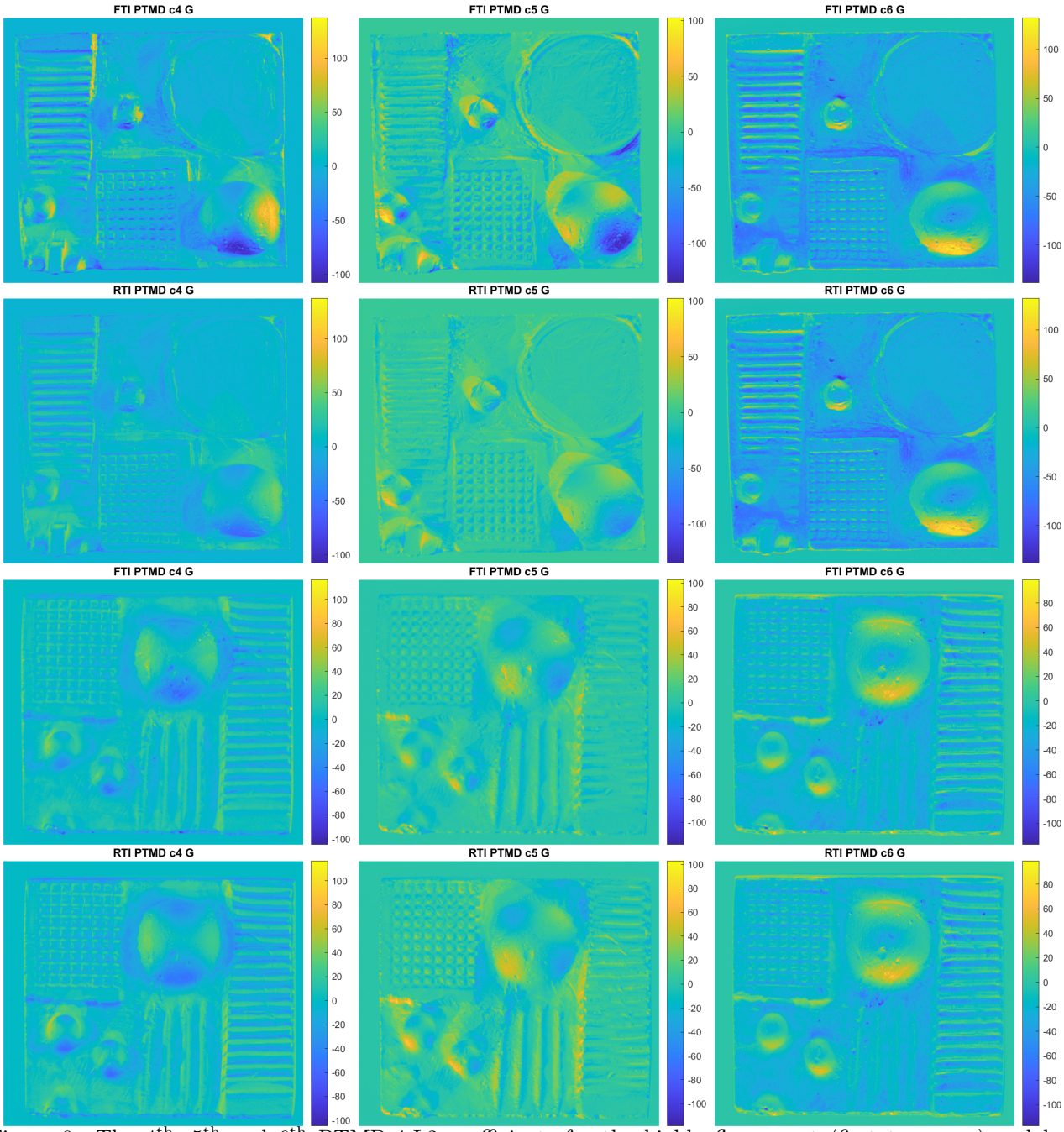

Figure 9: The 4^{th}, 5^{th} and 6^{th} PTMD-4-L2 coefficients for the highly fluorescent (first two rows) and low fluorescent (last two rows) mockups, plotted for the Green color channel, in both visible and fluorescence modes. These coefficients model the non-Lambertian behaviour as encoded by the quadratic and constant terms of the second-order polynomial, as expressed in Eq. 3. Overall, the highest difference between RTI and FTI is registered by coefficients 4 and 5, while the constant term stays invariant.

5. CONCLUSION

In this work, the estimation of normal and appearance maps of heterogeneous fluorescent scenes with non-flat geometries and multiple objects have been investigated under a Reflectance and Fluorescence Transformation Imaging setup. Through qualitative and quantitative analysis of the normal vectors recovered with first and second-order polynomial models, it was shown that contrary to the expectation given by the presumably ideal isotropic property of fluorescence, the surface reconstruction error was higher in the fluorescent mode than in the reflective visible mode. This might be due to the higher number of interreflections provoked by the luminescence becoming a secondary light that gets reflected by the object (that both reflects and re-emits the same color). Our findings show that is important to further investigate the appearance of complex fluorescent scenes with Fluorescence Transformation Imaging, going beyond the assumption of a perfectly Lambertian behaviour of luminescent materials. This is important for accurate appearance modelling and relighting of real-world fluorescent materials.

ACKNOWLEDGMENTS

We would like to acknowledge Giacomo Marchioro (University of Verona), who designed and manufactured the two fluorescent mockups, and helped with the data acquisition process.

REFERENCES

[1] Castro, Y., Pitard, G., Le Goïc, G., Brost, V., Mansouri, A., Pamart, A., Vallet, J.-M., and De Luca, L., "A new method for calibration of the spatial distribution of light positions in free-form rti acquisitions," in [*Optics for Arts, Architecture, and Archaeology VII*], **11058**, 1105813, International Society for Optics and Photonics (2019).

[2] Ponchio, F., Lamé, M., Scopigno, R., and Robertson, B., "Visualizing and transcribing complex writings through rti," in [*2018 IEEE 5th International Congress on Information Science and Technology (CiSt)*], 227–231, IEEE (2018).

[3] Vanweddingen, V., Vastenhoud, C., Proesmans, M., Hameeuw, H., Vandermeulen, B., Van der Perre, A., Lemmers, F., Watteeuw, L., and Van Gool, L., "A status quaestionis and future solutions for using multi-light reflectance imaging approaches for preserving cultural heritage artifacts," in [*Euro-Mediterranean Conference*], 204–211, Springer (2018).

[4] Irina, M. C., Tinsae, G. D., Andrea, G., Ruggero, P., Alberto, J.-V., and Enrico, G., "Artworks in the spotlight: characterization with a multispectral LED dome," *IOP Conference Series: Materials Science and Engineering* **364**, 012025 (June 2018).

[5] Kotoula, E. and Kyranoudi, M., "Study of ancient greek and roman coins using reflectance transformation imaging," *E-conservation magazine* **25**, 74–88 (2013).

[6] Kitanovski, V. and Hardeberg, J. Y., "Objective evaluation of relighting models on translucent materials from multispectral rti images," (2021).

[7] Kotoula, E. et al., "Reflectance transformation imaging beyond the visible: ultraviolet reflected and ultraviolet induced visible fluorescence," in [*Proceedings of the 43rd Annual Conference on Computer Applications and Quantitative Methods in Archaeology, Oxford*], 909–919 (2015).

[8] Treibitz, T., Murez, Z., Mitchell, B. G., and Kriegman, D., "Shape from fluorescence," in [*European Conference on Computer Vision*], 292–306, Springer (2012).

[9] Sato, I., Okabe, T., and Sato, Y., "Bispectral photometric stereo based on fluorescence," in [*2012 IEEE Conference on Computer Vision and Pattern Recognition*], 270–277 (Jun 2012).

[10] Woodham, R. J., "Photometric stereo: A reflectance map technique for determining surface orientation from image intensity," in [*Image Understanding Systems and Industrial Applications I*], **155**, 136–143, International Society for Optics and Photonics (1979).

[11] Malzbender, T., Gelb, D., and Wolters, H., "Polynomial texture maps," in [*Proceedings of the 28th annual conference on Computer graphics and interactive techniques*], 519–528 (2001).

[12] Drew, M. S., Hel-Or, Y., Malzbender, T., and Hajari, N., "Robust estimation of surface properties and interpolation of shadow/specularity components," *Image and Vision Computing* **30**(4-5), 317–331 (2012).

[13] Ikehata, S., Wipf, D., Matsushita, Y., and Aizawa, K., "Robust photometric stereo using sparse regression," in [*2012 IEEE Conference on Computer Vision and Pattern Recognition*], 318–325, IEEE (2012).
[14] Wu, L., Ganesh, A., Shi, B., Matsushita, Y., Wang, Y., and Ma, Y., "Robust photometric stereo via low-rank matrix completion and recovery," in [*Asian Conference on Computer Vision*], 703–717, Springer (2010).
[15] Tominaga, S., Hirai, K., and Horiuchi, T., "Measurement and modeling of bidirectional characteristics of fluorescent objects," in [*International Conference on Image and Signal Processing*], 35–42, Springer (2014).
[16] Fu, Y., Lam, A., Matsushita, Y., Sato, I., and Sato, Y., "Interreflection removal using fluorescence," in [*European Conference on Computer Vision*], 203–217, Springer (2014).
[17] Ciortan, I. M., Pintus, R., Marchioro, G., Daffara, C., Giachetti, A., and Gobbetti, E., "A Practical Reflectance Transformation Imaging Pipeline for Surface Characterization in Cultural Heritage," in [*Eurographics Workshop on Graphics and Cultural Heritage*], Catalano, C. E. and Luca, L. D., eds., The Eurographics Association (2016).
[18] "Rtitool." https://github.com/giach68/RTITool/. (Accessed on 2021-05-30).
[19] "Gocator 3210 large field of view 3d snapshot sensor." https://lmi3d.com/series/gocator-3210/. (Accessed on 2021-05-30).
[20] Corsini, M., Dellepiane, M., Ponchio, F., and Scopigno, R., "Image-to-geometry registration: a mutual information method exploiting illumination-related geometric properties," in [*Computer Graphics Forum*], **28**(7), 1755–1764, Wiley Online Library (2009).
[21] Cignoni, P., Ranzuglia, G., Callieri, M., Corsini, M., Ganovelli, F., Pietroni, N., and Tarini, M., "Meshlab," (2011).
[22] Nimier-David, M., Vicini, D., Zeltner, T., and Jakob, W., "Mitsuba 2: A retargetable forward and inverse renderer," *ACM Transactions on Graphics (TOG)* **38**(6), 1–17 (2019).
[23] Shi, B., Wu, Z., Mo, Z., Duan, D., Yeung, S.-K., and Tan, P., "A benchmark dataset and evaluation for non-lambertian and uncalibrated photometric stereo," in [*Proceedings of the IEEE Conference on Computer Vision and Pattern Recognition*], 3707–3716 (2016).
[24] Shi, B., Mo, Z., Wu, Z., Duan, D., Yeung, S.-K., and Tan, P., "A benchmark dataset and evaluation for non-lambertian and uncalibrated photometric stereo," *IEEE Transactions on Pattern Analysis and Machine Intelligence* **41**(2), 271–284 (2019).

APPENDIX A. ANGULAR DIFFERENCE MAPS

Angular differences maps between normals from all models and light configurations (Lc) with respect to ground truth are presented on a scale from 0° to 40° for the highly fluorescent and low fluorescent mockups.

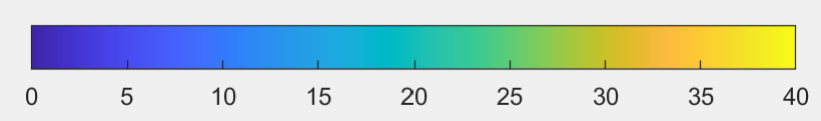

FTI PS-L2 Lc1

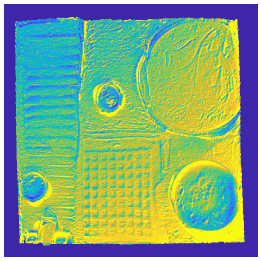

FTI PS-L2 Lc2

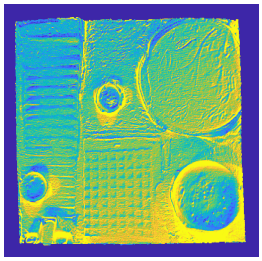

FTI PS-L2 Lc3

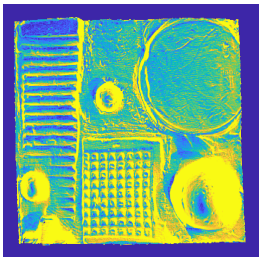

FTI PS-L2 Lc4

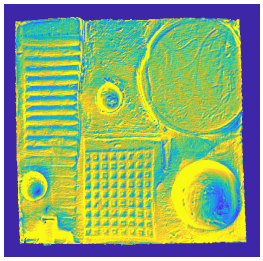

RTI PS-L2 Lc1

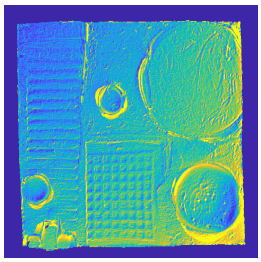

RTI PS-L2 Lc2

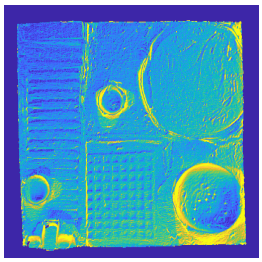

RTI PS-L2 Lc3

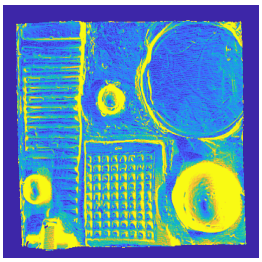

RTI PS-L2 Lc4

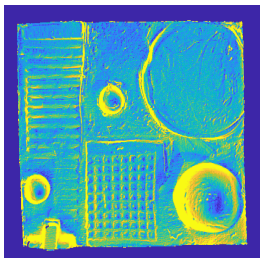

FTI PS4-L2 Lc1

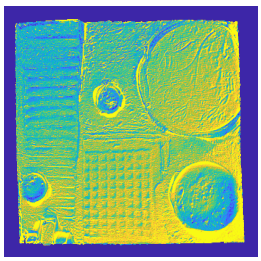

FTI PS4-L2 Lc2

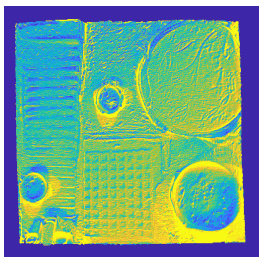

FTI PS4-L2 Lc3

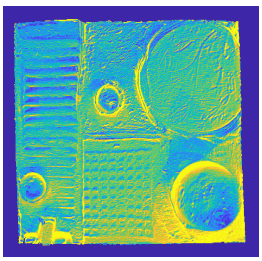

FTI PS4-L2 Lc4

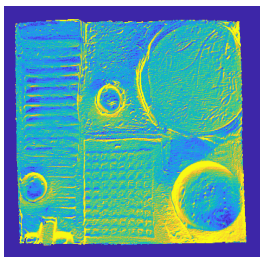

RTI PS4-L2 Lc1

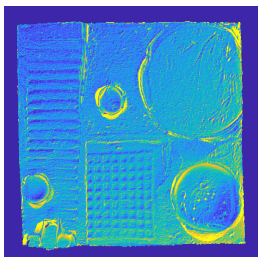

RTI PS4-L2 Lc2

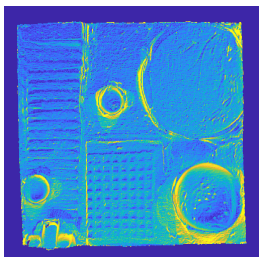

RTI PS4-L2 Lc3

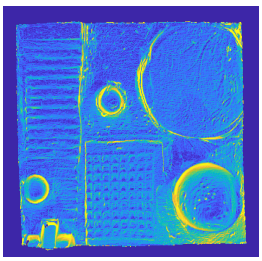

RTI PS4-L2 Lc4

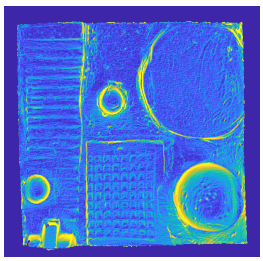

FTI PS-L2 Lc1

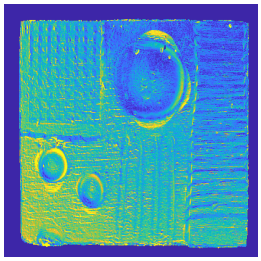

FTI PS-L2 Lc2

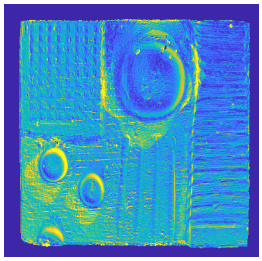

FTI PS-L2 Lc3

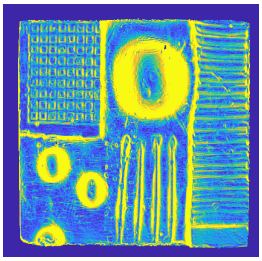

FTI PS-L2 Lc4

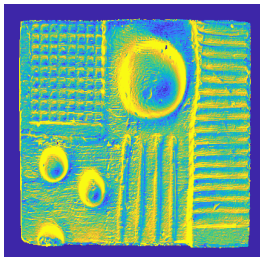

RTI PS-L2 Lc1

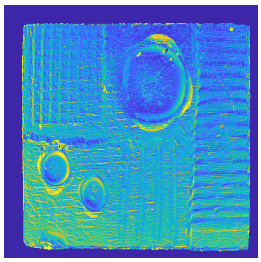

RTI PS-L2 Lc2

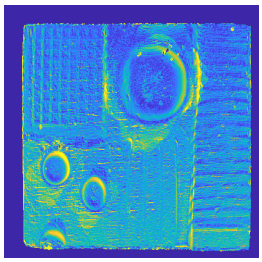

RTI PS-L2 Lc3

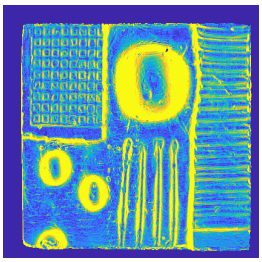

RTI PS-L2 Lc4

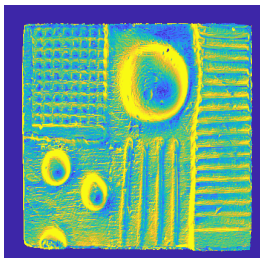

FTI PS4-L2 Lc1

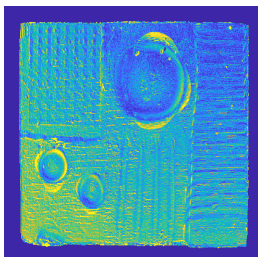

FTI PS4-L2 Lc2

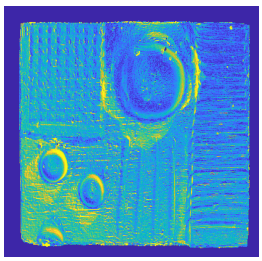

FTI PS4-L2 Lc3

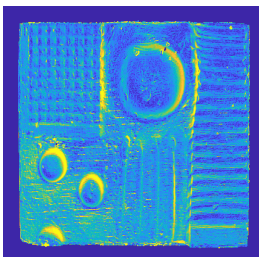

FTI PS4-L2 Lc4

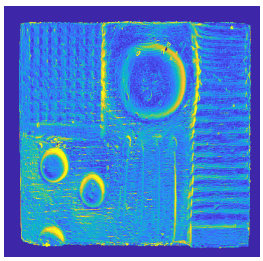

RTI PS4-L2 Lc1

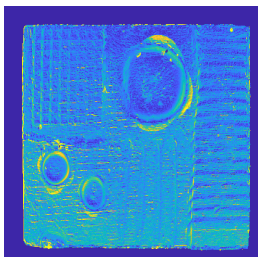

RTI PS4-L2 Lc2

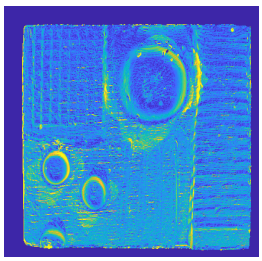

RTI PS4-L2 Lc3

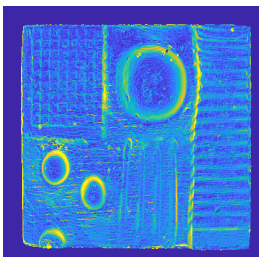

RTI PS4-L2 Lc4

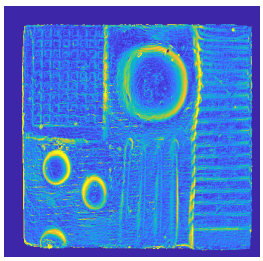

FTI PS-RPCA Lc1

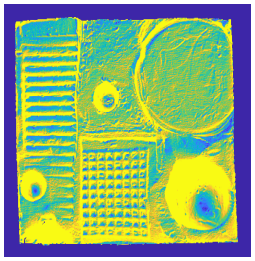

FTI PS-RPCA Lc2

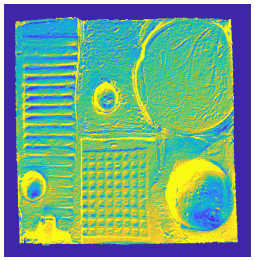

FTI PS-RPCA Lc3

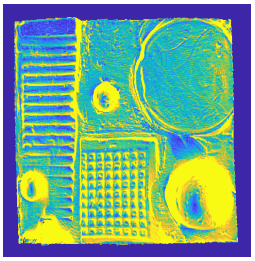

FTI PS-RPCA Lc4

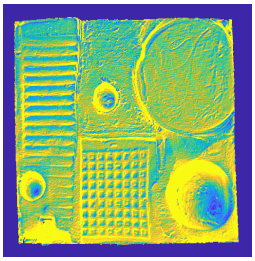

RTI PS-RPCA Lc1

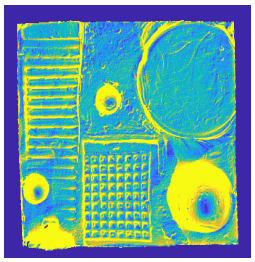

RTI PS-RPCA Lc2

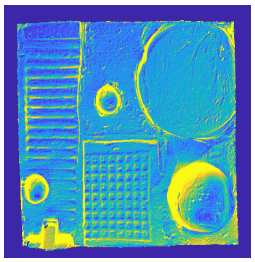

RTI PS-RPCA Lc3

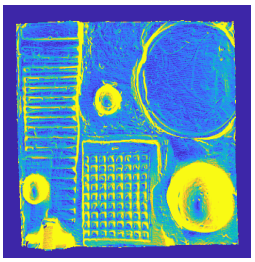

RTI PS-RPCA Lc4

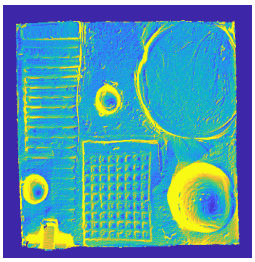

FTI PS-RPCA Lc1

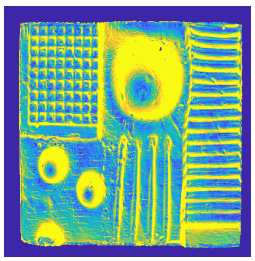

FTI PS-RPCA Lc2

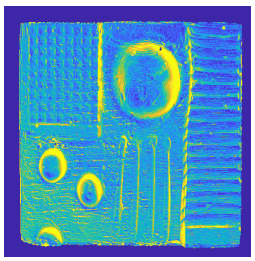

FTI PS-RPCA Lc3

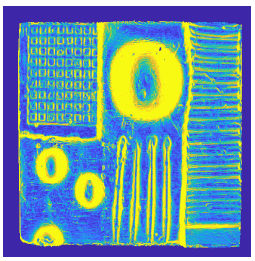

FTI PS-RPCA Lc4

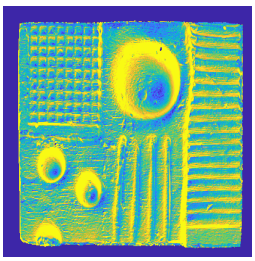

RTI PS-RPCA Lc1

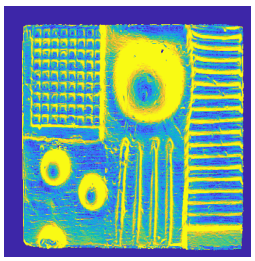

RTI PS-RPCA Lc2

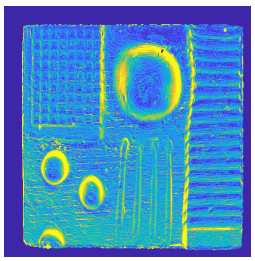

RTI PS-RPCA Lc3

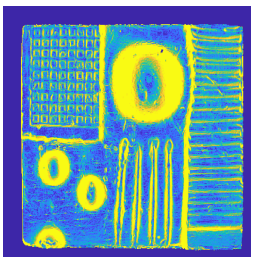

RTI PS-RPCA Lc4

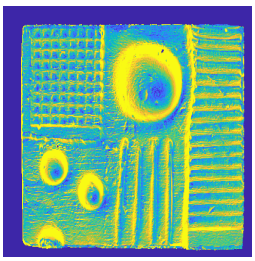

FTI PTMD-4-L2 Lc2

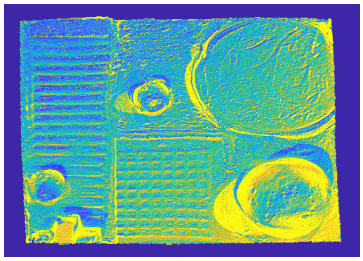

FTI PTMD-4-L2 Lc3

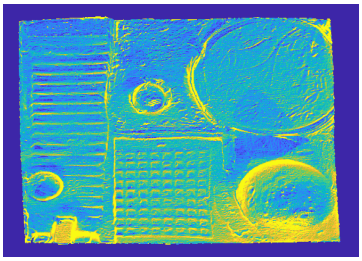

FTI PTMD-4-L2 Lc4

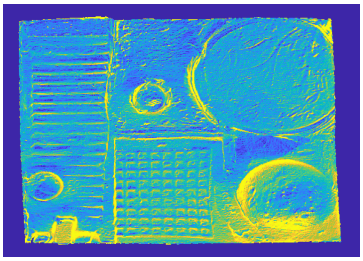

RTI PTMD-4-L2 Lc2

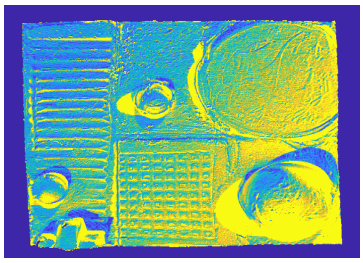

RTI PTMD-4-L2 Lc3

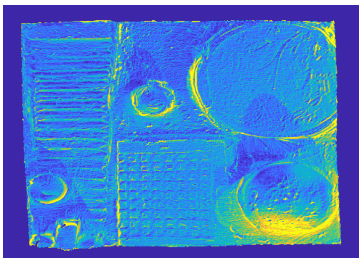

RTI PTMD-4-L2 Lc4

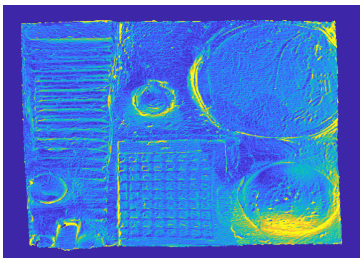

FTI PTMD-4-L2 Lc2

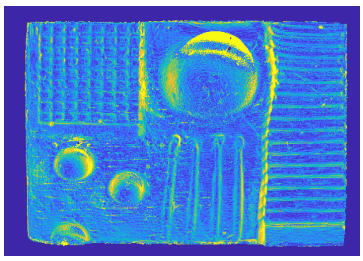

FTI PTMD-4-L2 Lc3

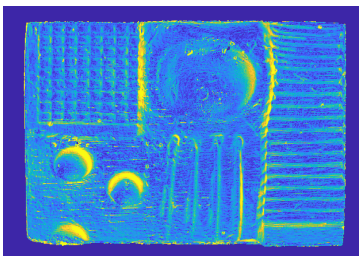

FTI PTMD-4-L2 Lc4

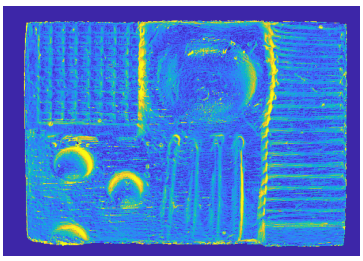

RTI PTMD-4-L2 Lc2

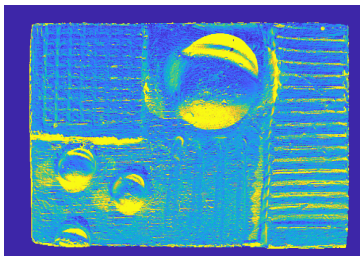

RTI PTMD-4-L2 Lc3

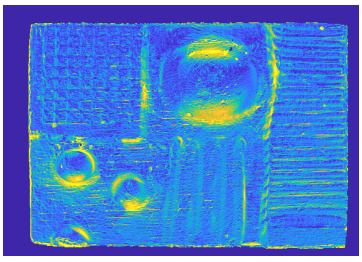

RTI PTMD-4-L2 Lc4